INTERNATIONAL JOURNAL
OF
PHARMACEUTICAL SCIENCES
AND
RESEARCH

MOLECULAR DOCKING AND 3D-QSAR ANALYSIS STUDIES OF MMP-12 INHIBITORS

Shravan Kumar Gunda [1]*, Lokesh Kumar Akula [1], Salwa Shaik [2], Seshagiri Bandi [1] and Mahmood Shaik[1]

Division of Bioinformatics [1], Osmania University, Hyderabad 500007, Andhra Pradesh, India
Dept. of Mechanical Engineering [2], CVSR College, Ghatkesar, RR district, Telangana, India

ABSTRACT: Matrix metalloproteinase 12 (MMP-12) inhibitors is an important research topic because of its wide range of associated health implications. The interaction mode of a series of pyridinone compounds with MMP-12 has been studied using molecular docking and 3D-QSAR approaches. Flexible docking was used for the determination of active conformation and molecular alignment. Comparative molecular field analysis (CoMFA) and comparative molecular similarity indices analysis (CoMSIA) were used to develop 3D-QSAR models of 64 pyridinone-based compounds. The q^2 values were 0.552 and 0.542 for both CoMFA and CoMSIA models, respectively. The ability of these models was validated by 16 compounds of the test set. The resulting contour maps produced by the best CoMFA and CoMSIA models were used to identify the structural features relevant to the biological activity in this series of compounds. FlexX were employed to dock the inhibitors into the active site of the MMP-12 and these docking studies revealed the vital interactions and binding conformation of the inhibitors. The results demonstrate that combination of ligand-based and receptor-based modeling is a powerful approach to Build 3D-QSAR models.

INTRODUCTION: Matrix metalloproteinases (MMPs, EC 3.4.24), also called matrixins, are a family of structurally related zinc- and calcium-dependent endopeptidases. They degrade the extracellular matrix (ECM) of connective tissues and basement membranes. ECM is essential for the function of almost any cell type and its components provide a structural lattice to which cells may adhere, facilitating their organization in the tissue. Extracellular matrix components include structural proteins like collagen and various adhesion proteins (elastin, fibronectin, laminin and proteoglycan) [1]. Collagens are a family of proteins with 29 known members; even if not all are found in the ECM [2], they share a common structural motif of helical fibrils.

The tropocollagen or collagen molecule (~1400 amino acids, 300 nm in length, 1.5 nm in diameter) is a subunit of larger fibrils, collagen aggregates. It is made up of three polypeptide strands with the conformation of a left-handed helix twisted together into a triple helix or "super helix".

Elastin is responsible for the flexibility of tissues, particularly in blood vessels, lungs, skin, and ligamentum nuchae. Tropoelastin protein subunits (~830 amino acids) are linked together to give the elastin fibre [3]. Fibronectin is an adhesive glycoprotein which binds multiple ECM factors and plays important roles in cell adhesion, migration, growth and differentiation [4].

It exists as a dimer, consisting of two identical monomers linked by disulphide bonds [5]. Each monomer is composed of types I, II, and III repeating units. Two intra molecular disulphide bonds within each type I and type II module stabilize the folded structure [6]. These modules are

organized into binding sites for collagen, integrins and other extracellular molecules.

The extracellular matrix is not only a support for cells, but it is also implicated in cell-cell interactions, invasion, cell migration and proliferation. Matrix metalloproteinases, degrading structural components of the ECM, regulate the tissue architecture and cellular signaling [7]. They participate in physiological processes such as morphogenesis, embryogenesis, angiogenesis, ovulation, postpartum and post-lactational involution, differentiation, inflammation, bone resorption and wound healing [8]. In pathological conditions, this balance is shifted towards over activation of MMPs leading to excessive degradation of the matrix components.

Excessive MMP activity has been implicated in numerous disease states involving matrix degradation, which include arthritis [9], periodontal diseases [10], osteogenesis imperfecta, Alzheimer's disease [11] and osteoarthritis, osteoporosis, cardiovascular disease, inflammatory diseases, neuro inflammation, asthma, fibrosis, atherosclerosis, multiple sclerosis, aortic aneurysms, tumorigenesis and cancer progression (metastasis, angiogenesis and invasion).

In our ongoing project, further structural modification will be carried out as suggested by the quantitative structural activity relationship, which has been widely used in pharmacology in attempts to optimize drug compounds and molecular docking can fit molecules together in a favorable configuration to form a complex system. Therefore, 3D-QSAR and interaction mode of these series of pyridinone derivatives will be of benefit for us to develop new potent MMP-12 inhibitors. Herein, 3D-QSAR studies of 64 pyridinone derivatives using CoMFA and CoMSIA along with FlexX docking method are described.

MATERIALS AND METHODS:
Data sets and biological activity:
The molecular modeling studies were carried out using Sybyl 6.7. The initial structures were minimized at Tripos force field [12] with Gasteiger-Huckel charges by using Powell gradient method, and convergence criterion was 0.05kcal/mol. The

dataset for the CoMSIA [13] and CoMFA [14] calculations consisted of compounds that had been taken from the literature [15]. From the original 67 compounds, 3 compounds (41, 60 and 61) were removed because they have either undefined activity or stereochemistry. Forty eight compounds were randomly selected as the training set and the remaining [16] compounds used as test set. The biological data obtained as IC_{50} were converted to pIC_{50} ($-logIC_{50}$) values and used as dependent variables in the 3D-QSAR analysis.

Molecular modeling and alignment:
CoMFA and CoMSIA results may be extremely sensitive to a number of factors such as alignment, over all orientation of the aligned molecules, lattice shifting step size and probe atom type. The accuracy of CoMFA and CoMSIA model prediction and the reliability of the contour models depend strongly on the structural alignment of the molecules and thus we applied molecular alignment to align all the molecules used in present study in space. The molecular alignment was achieved by SYBYL routine align database.

The initial structures were minimized at tripos force field with Gasteiger-Hückel charges using conjugate gradient method, and convergence criterion was 0.05kcal/mol. The most active compound 16 was used as an alignment template and the rest of the molecules were aligned to it by using the common substructure as shown in **Fig. 1**.
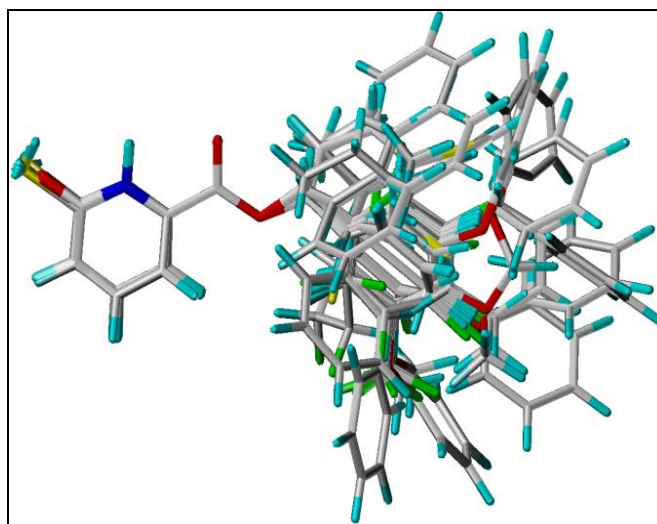

FIG. 1: STRUCTURAL ALIGNMENT OF THE COMPOUNDS IN THE TRAINING SET AND TEST SET FOR CONSTRUCTING 3D-QSAR COMFA AND COMSIA MODELS

CoMFA studies:

Steric and electrostatic interactions were calculated using the tripo's force field with a distance-dependent dielectric constant at all interactions in a regularly spaced (2Å) grid taking a sp^3 carbon atom as steric probe and a+1 charge as electrostatic probe. The cutoff value was set to 30kcal/mol for both steric and electrostatic fields. The CoMFA regression analysis was carried out using the full cross-validated partial least squares method (leave-one-out). The minimum sigma (column filtering) was set to 2.0kcal/mol. It is used improve the signal to noise ratio by omitting those lattice points whose energy variation was below this threshold level. The final evaluated model, non cross-validated conventional regression, was developed with the optimum number of components to yield a non cross-validated r^2 value [16].

CoMSIA studies:

In CoMSIA, a distance-dependent Gaussian-type physicochemical property has been adopted to avoid singularities at the atomic positions and dramatic changes of potential energy for grids being in the proximity of the surface. By using standard parameters and no arbitrary cutoff limits, five fields associated to five physicochemical properties, namely, steric, electrostatic, hydrophobic, H donor and acceptor were calculated. The steric field contribution was reflected by the third power of the atomic radii of the atoms. The electrostatic properties were introduced as atomic charges resulting from docking. In general, molecular similarity indices analysis, $A_{F,K}$, between the compounds of interest were computed by placing a probe atom at the intersections of the lattice points and using Equation (1).

$$A^q_{F,K}(j) = -\Sigma\ W_{probe,k}\ W_{ik}\ e^{-a r^2_{iq}} \qquad (1)$$

where q represents a grid point, i is the summation index over all atoms of the molecule j under computation, W_{ik} is the actual value of the physicochemical property k of atom i, and $W_{probe,k}$ is the value of the probe atom. In the present study, we used a probe atom ($W_{probe,k}$) with charge +1, radius 1Å, hydrophobicity +1,and attenuation factor of 0.3 for the Gaussian type distance. The statistical evaluation for the CoMSIA analysis was performed in the same way as described for CoMFA.

Partial Least Squares (PLS) analysis:

Partial least square (PLS) [17] methods were used to linearly correlate the CoMFA and CoMSIA fields to biological activity values. The conventional cross-validation was performed using leave-one-out (LOO) method in which one compound is removed from the dataset and its activity is predicted using the model derived from the rest of the molecules used in the dataset.

For CoMFA Equal weights were assigned to steric and electrostatic fields using CoMFA STD scaling option. To improve and speed up the analysis and reduce noise, minimum column filtering value of 2.0kcal/mol was used for the cross-validation. Calculated conventional r^2 by performing Non-cross-validation with the same number of components. To assess the robustness and statistical confidence of the derived models bootstrapping analysis for 100 runs was performed [18]. Bootstrapping involves the generation of many new data sets from original data set and is obtained by randomly choosing samples from the original data set.

The difference between the parameters calculated from the original data set and the average of the parameters calculated from the many bootstrapping samplings is a measure of the bias of the original calculations.

Molecular Docking:

The docking studies were carried out using the FlexX program [19] interfaced with Sybyl 6.7. In FlexX automated docking program, the ligand is considered as flexible, while the protein is considered as a rigid structure. The ligand is built in an incremental fashion, where each new fragment is added in all possible positions and conformations to a pre-placed base fragment inside the active site.

All the molecules for docking were sketched in the SYBYL and minimized using PM3 method and all the charges were removed [20]. The 3D coordinates of the active sites were taken from the X-ray crystal structures of the MMP-12 (Alternate name:

Fibroblast collagenase) were obtained from protein databank (PDB ID: 1HFC). The PDB file obtained from protein data bank was used as a receptor site. Removed all water molecules and the protein was modified to dock inhibitor and also hydrogens were added. The active site was defined with a distance of 6.5 Å around the co-crystallized ligand. Formal charges were assigned to all the molecules and FlexX run was submitted.

RESULTS AND DISCUSSION:
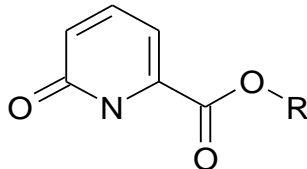### 3D-QSAR analysis:
CoMFA analysis:
The major objective of CoMFA analysis for the pyridinone-based derivatives was to find the best predictive model within the system. We picked up total 64 pyridinone inhibitors for CoMFA analyses, in which 48 compounds were training set and the other 16 as test set compounds for model validation. The data for predicted values versus experimental results are resulted in **Table 1**. The PLS analysis results CoMFA are summarized in

Table 2, which shows that all of the statistical indexes are reasonably high, and the relationship between experimental binding affinities (-log IC_{50}) and predicted activities by the CoMFA model is presented in **Figure 3a.**

As listed in **Table 2,** the ligand-based alignment gave better results for CoMFA model using both field descriptors with leave-one-out q^2 of 0.552, cross-validated q^2 of 0.555. The non cross-validated PLS analysis with the optimum components revealed a conventional r^2 value of 0.827, with a F-value (Fisher ratio) of 40.124 and an estimated standard error of estimate (SEE) equal to 0.089

These values indicate that the CoMFA model has a good conventional statistical correlation and a fair predictive ability. The percentage of the variance explained by steric and electrostatic field descriptors are 42.4 and 57.6 respectively.

TABLE 1: EXPERIMENTAL AND PREDICTED PIC$_{50}$ VALUES FOR TRAINING AND TEST SET MOLECULES ALONG WITH THEIR DOCKING SCORES

C.No	R group	pIC$_{50}$	CoMFA Predicted	CoMFA Residual	CoMSIA Predicted	CoMSIA Residual	Dock score
1	Isopropyl	4.17	4.113	0.057	4.177	-0.007	-23.5
2	Cyclobutyl	4.29	4.137	0.153	4.142	0.148	-26.9
3	CH$_2$CHC(CH$_3$)$_2$	4.17	4.107	0.063	4.093	0.077	-24.8
4	CH$_2$CCCH$_3$	4.15	4.229	-0.079	4.224	-0.074	-24.2
5	Cyclohexyl	4.15	4.204	-0.054	4.274	-0.124	-24.9
6	Benzyl	4.16	4.143	0.017	4.184	-0.024	-24.2
7	(CH$_2$)$_2$C$_6$H$_5$	4.16	4.193	-0.033	4.193	-0.033	-27.6
8	4-Me-Benzyl	4.16	4.176	-0.016	4.185	-0.025	-25.1
9	3-CF$_3$-Benzyl	4.08	4.187	-0.107	4.236	-0.156	-25.5
10	3-CF=-Benzyl	4.19	4.093	0.097	4.170	0.020	-27.1
11	3-OMe-Benzyl	4.16	4.266	-0.106	4.273	-0.113	-25.2
12*	4-OMe-Benzyl	3.97	4.310	-0.340	4.260	-0.290	-24.3
13	(CH$_2$)$_4$OC$_6$H$_4$	4.10	4.075	0.025	4.171	-0.071	-24.7
14	(CH$_2$)$_4$OC$_6$H$_4$	4.08	4.118	-0.038	4.104	-0.024	-24.2
15	2-F-Benzyl	4.16	4.296	-0.136	4.240	-0.080	-25.2
16	3-F-Benzyl	4.80	4.415	0.385	4.408	0.392	-25.2
17	4-F-Benzyl	4.18	4.413	-0.233	4.349	-0.169	-24.4
18	2,6-F-Benzyl	4.22	4.301	-0.081	4.272	-0.052	-24.3
19*	2,5-F-Benzyl	4.00	4.280	-0.280	4.240	-0.240	-25.3
20	3,5-F-Benzyl	4.70	4.498	0.202	4.452	0.248	-24.4
21	2,4,6-F-Benzyl	4.50	4.160	0.340	4.116	0.384	-24.6
22	2,4,5-F-Benzyl	4.25	4.351	-0.101	4.290	-0.040	-25.4
23	CH$_2$C$_6$H$_5$	4.20	4.348	-0.148	4.312	-0.112	-23.5
24*	2-Cl-Benzyl	4.16	4.270	-0.110	4.270	-0.110	-25.0
25	3-Cl-Benzyl	4.34	4.547	-0.207	4.565	-0.225	-24.5

26	4-Cl-Benzyl	4.32	4.311	0.009	4.263	0.057	-23.6
27	2-Br-Benzyl	4.35	4.243	0.107	4.230	0.120	-25.5
28	2-Br-Benzyl	4.50	4.378	0.122	4.516	-0.016	-23.5
29*	2-Br-Benzyl	3.98	4.270	-0.290	4.250	-0.270	-25.3
30	Cinnamyl	4.15	4.229	-0.079	4.271	-0.121	-25.7
31*	1-Napthalyl	3.95	4.340	-0.390	4.220	-0.270	-24.6
32*	2-Napthalyl	4.01	4.200	-0.190	4.130	-0.120	-25.9
33	Piperonyl	3.98	4.139	-0.159	4.129	-0.149	-26.4
34	3-Ph-Benzyl	4.00	3.969	0.031	3.938	0.062	-25.4
35*	3-Oph-Benzyl	3.92	4.370	-0.450	4.440	-0.520	-25.0
36	2-Thiophenyl	4.18	4.320	-0.140	4.315	-0.135	-25.0
37	3-Thiophenyl	4.20	4.390	-0.190	4.196	0.004	-32.7
38	2-Furyl	4.11	4.195	-0.085	4.204	-0.094	-24.2
39	$(CH_2)_4CH_3$	4.16	4.117	0.043	4.161	-0.001	-25.1
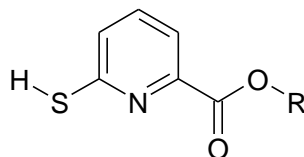
C No	R group	pic_{50}	CoMFA		CoMSIA		Dock score
			Predicted	Residual	Predicted	Residual	
40	Isopropyl	3.83	3.965	-0.135	3.948	-0.118	-10.0
42*	Cyclohexyl	4.06	3.890	0.170	3.920	0.140	-8.9
43	Benzyl	4.08	3.772	0.308	3.861	0.219	-10.1
44	$(CH_2)_2C_6H_5$	3.93	3.978	-0.048	4.089	-0.159	-14.4
45*	$(CH_2)_2C_6H_5$	4.07	3.860	0.210	3.850	0.220	-15.9
46*	3-Me-Benzyl	4.15	3.780	0.370	3.850	0.300	-16.2
47*	4-Me-Benzyl	4.09	3.780	0.310	3.810	0.280	-13.6
48	$3-CF_3$-Benzyl	3.87	3.854	0.016	3.725	0.145	-17.3
49	$4-CF_3$-Benzyl	4.02	3.911	0.109	3.886	0.134	-15.3
50*	3-OMe-Benzyl	4.10	3.870	0.230	3.850	0.250	-16.1
51	4-OMe-Benzyl	4.01	3.804	0.206	3.727	0.283	-16.4
52*	$(CH_2)_4OC_6H_5$	4.10	3.710	0.390	3.720	0.380	-18.0
53	3-F-Benzyl	3.82	4.174	-0.354	4.105	-0.285	-19.0
54	4-F-Benzyl	3.95	3.843	0.107	3.944	0.006	-16.6
55	2,6-F-Benzyl	3.89	3.984	-0.094	3.968	-0.078	-16.8
56*	2,5-F-Benzyl	4.76	3.922	0.838	3.923	0.837	-10.4
57	2,4,5-F-Benzyl	3.97	3.930	0.040	3.920	0.050	-14.6
58	$CH_2C_6F_6$	4.09	4.228	-0.138	4.424	-0.334	-19.9
59	4-Cl-Benzyl	3.93	3.987	-0.057	3.995	-0.065	-15.1
62	2-Napthalyl	3.99	4.152	-0.162	4.022	-0.032	-14.4
63	1-Napthalyl	3.86	3.889	-0.029	3.933	-0.073	-21.1
64*	4-Ph-Benzyl	4.28	3.860	0.420	3.760	0.520	-19.1
65*	3-Ph-Benzyl	4.14	3.820	0.320	3.790	0.350	-11.5
66	3-OPh-Benzyl	3.96	3.878	0.082	3.848	0.112	-12.6
67	4-OPh-Benzyl	4.03	3.862	0.168	3.839	0.191	-16.1

Test set compounds are represented by bold * mark

CoMSIA analysis:

Using steric, electrostatic, hydrophobic, and hydrogen bond donor and acceptor properties as descriptors, CoMSIA analysis was performed. The results are listed in **Table 2**, where the best q^2 was found by using all five different descriptor variables. This demonstrates that these variables are necessary to describe the interaction mode of the pyridinone inhibitors with MMP-12, as well as the field properties around the inhibitors. The

predicted binding affinities derived from CoMSIA analysis are also listed in **Table 1** and shown in **Fig.3b.** The CoMSIA study revealed leave-one-out q^2= 0.542, cross-validated q^2= 0.550, non-cross-validated r^2= 0.825, SEE 0.090 and F = 32.312. The percentage of the variance explained by steric, electrostatic, hydrophobic, hydrogen bond donor, and hydrogen bond acceptor field descriptors are 13.3, 44.2, 24.3, 5.4 and 12.8 respectively.

TABLE 2: PLS STATISTICS OF CoMFA MODEL

Component	CoMFA	CoMSIA
q^2	0.552	0.542
r^2	0.827	0.825
N	5	6
F-Value	40.124	32.312
SEE	0.089	0.090
Cross validation	0.555	0.550
Field Contribution (%)		
Steric	42.4	13.3
Electrostatic	57.6	44.2
Hydrophobic	-	24.3
Hydrogen bond donor	-	5.4
Hydrogen bond acceptor	-	12.8
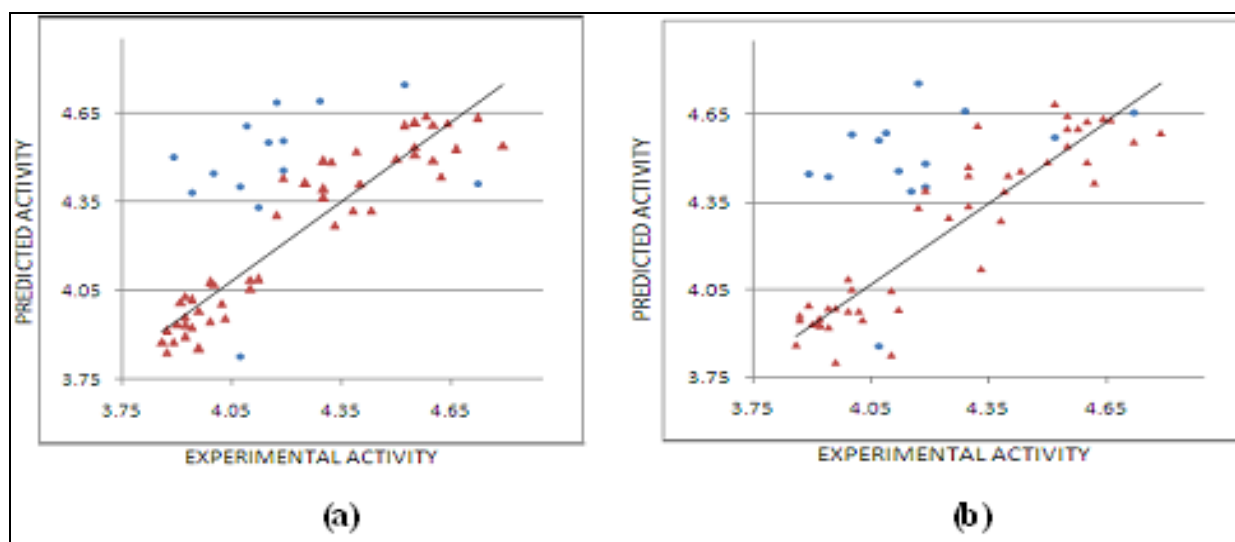
FIG. (3a) PREDICTED ACTIVITIES (PA) BY CoMFA MODEL VERSUS EXPERIMENTAL ACTIVITIES (EA) OF *PYRIDINONES*. FILLED TRIANGLES INDICATE COMPOUNDS OF THE TRAINING SET; FILLED CIRCLES INDICATE COMPOUNDS OF THE TEST SET. (3b) PREDICTED ACTIVITIES (PA) BY CoMSIA MODEL VERSUS EXPERIMENTAL ACTIVITIES (EA) OF *PYRIDINONES*. FILLED TRIANGLES INDICATE COMPOUNDS OF THE TRAINING SET; FILLED CIRCLES INDICATE COMPOUNDS OF THE TEST SET

CoMFA and CoMSIA contour analysis:
The CoMFA steric and electrostatic fields from the final non-cross-validated were plotted as 3-D contour maps (**Fig. 4**). The field energies at each lattice point were calculated as the scalar results of the coefficient and the standard deviation associated with a particular column of the data table (SD* coeff), always plotted as the percentages of the contributions of CoMFA equation.

These maps show regions where differences in molecular fields are associated with differences in biological activity. **Fig. 4** represents the CoMFA steric and electrostatic contours, while those of CoMSIA steric, electrostatic, hydrophobic, H bond donor and H bond acceptor are shown in **Fig. 5,** respectively. In the contour maps, each of the colored contour map represents particular properties such as green contours for regions of high steric tolerance (80% contribution), yellow for low steric tolerance (20% contribution), red color contours for regions of decreased electrostatic tolerance for positive charge (20% contribution), blue regions for decreased electrostatic tolerance for negative charge (80% contribution).

The yellow contours represent hydrophobically favored regions (80% contribution) and white contours for hydrophobically disfavored regions (20% contribution). The magenta and red contours denote favorable and unfavorable regions for H bond acceptor, respectively whereas cyan and purple contours represents favorable and unfavorable regions for H bond donor groups, respectively.

The CoMFA steric and electrostatic contour maps are shown in Fig. 4a and 4b, respectively, the green steric regions are present as large regions near the side chain for the most active compound 16, which indicates that substitution of bulky group at these positions would help increase potency.

Another group of sterically large disfavored yellow regions are present near the pyridine ring and at the R side chain, above the benzyl ring, compounds having bulky substituent's at this position are hence less active, for example low potency of most compounds (6, 15-22, 26, 53-57) might be attributed to the presence of substitutions attached to the yellow contours present at the side chain R. This indicates that removal of bulky groups from the side chains will enhance the activity of these compounds.
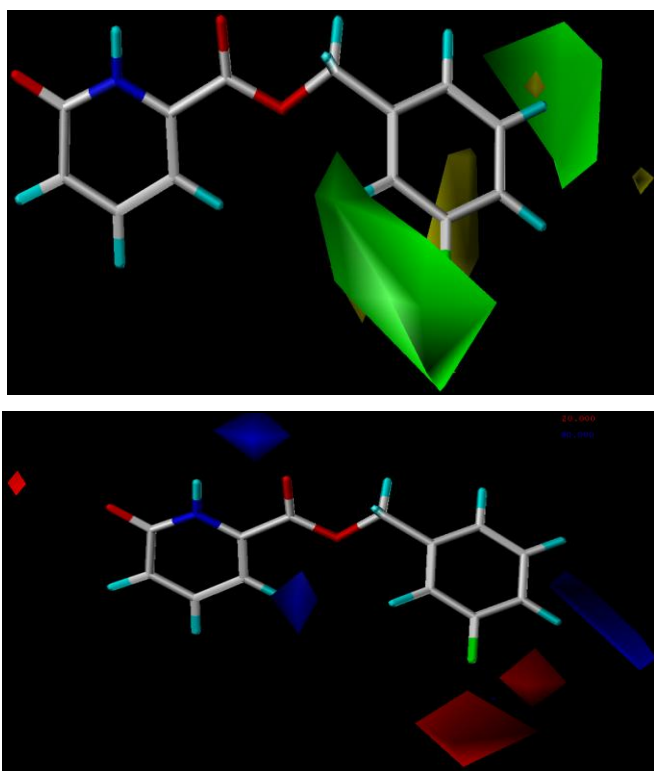

FIG. 4: CoMFA CONTOUR MAPS ARE SHOWN IN THE PRESENCE OF THE MOST POTENT COMPOUND 16. (a) STERIC FIELDS: GREEN INDICATES REGIONS WHERE BULKY GROUPS INCREASE ACTIVITY, WHEREAS YELLOW INDICATE REGIONS WHERE BULKY GROUPS DECREASE ACTIVITY. (b) ELECTROSTATIC FIELDS: BLUE INDICATES REGIONS WHERE MORE POSITIVELY CHARGED GROUPS INCREASE ACTIVITY, WHEREAS RED INDICATES REGIONS WHERE MORE NEGATIVELY CHARGED GROUPS INCREASE ACTIVITY.

The COMFA electrostatic contour plot is shown in Fig. 4b. The red regions near pyridine ring and near the -F group of side chain indicate that any electronegative group at this position would enhance the activity. Therefore compound 16 in which the benzyl group attached to the R side chain in contact with the red contour is more active than 1-5, 7, 23, 40-42, 59-63 wherein no such group is attached. Hence, substitution of electronegative group at these red contours near R side chain will enhance the activity of compounds.

Three blue contours are present in electrostatic contour map, one is in the place of side chain's benzyl ring and two blue contours are present in main ring below the pyridine ring and above the pyridine ring, indicate that substitution of electropositive group at this position would increase the activity. Hence 6, 9-15, 18-20, 24-28, 31, 44-51 with pyridine and benzyl rings pointing towards this blue contours have higher potency than compounds 2, 10, 16-17, 23, which either lack any electropositive group or in which it is farther from it.

Presence of blue contour below the pyridine ring determines that the electropositive environment is desirable at this position, hence electropositive environment -NH group occupying this position is present in all potent compounds.

The CoMSIA contour plots employing steric, electrostatic, hydrophobic, hydrogen bond donor and hydrogen bond acceptor are shown in **Fig.5**. The steric and electrostatic plots (**Fig. 5a and 5b**) show more variation from the corresponding CoMFA plots. It could be observed from **Fig 5a** that one green region and two yellow regions are spread across the benzyl ring of R group, which indicates that more bulky groups should be substituted near the green regions to enhance the activity and substitution of bulky group at this yellow regions might result in decrease of the activity.

Similar variation can also be observed from the CoMSIA plot (**Fig. 5b**), where only small regions of red and blue regions are present on the most active compound 16. The red regions present near the benzyl ring will enhance the activity by the substitution of electronegative groups, and a small blue contour present at the –NH group of pyridine

ring will increase the activity by the substitution of electropositive groups.
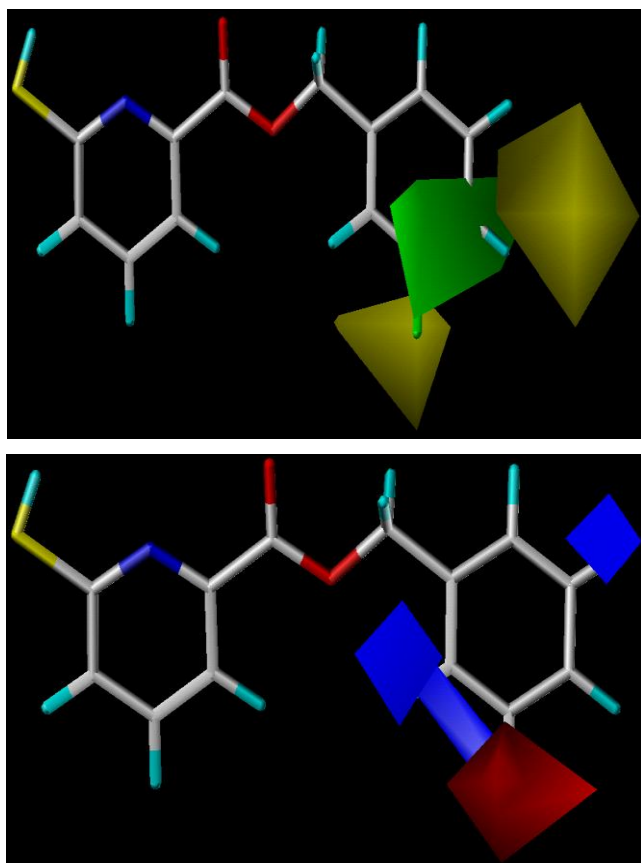

FIG. 5: COMSIA CONTOUR MAPS ARE SHOWN IN THE PRESENCE OF THE MOST POTENT COMPOUND 16. (A) STERIC FIELDS: GREEN INDICATES REGIONS WHERE BULKY GROUPS INCREASE ACTIVITY, WHEREAS YELLOW INDICATE REGIONS WHERE BULKY GROUPS DECREASE ACTIVITY. (B) ELECTROSTATIC FIELDS: BLUE INDICATES REGIONS WHERE MORE POSITIVELY CHARGED GROUPS INCREASE ACTIVITY, WHEREAS RED INDICATES REGIONS WHERE MORE NEGATIVELY CHARGED GROUPS INCREASE ACTIVITY.

In the CoMSIA hydrophobic contour maps, there were two yellow regions and two white regions close to the benzyl ring and one white region positioned at the pyridine ring. The two yellow regions present on the R side chain, indicates that any bulk group which is present at this position will represent the hydrophobically favored regions.

The large white region on the pyridine ring indicates that hydrophilic groups will be favorable, thus compounds that have an –NH group at that position will have much greater potency than those compounds without -NH group. Hydrogen-bond donor contour maps from CoMSIA are shown in **Fig. 5c**.
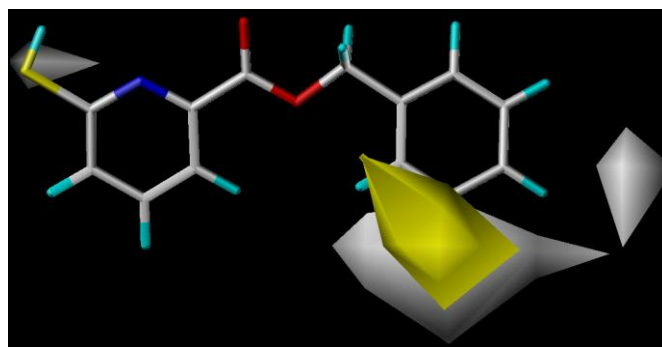

FIG .5c: CoMSIA CONTOUR MAPS ARE SHOWN IN THE PRESENCE OF THE MOST POTENT COMPOUND 16. YELLOW AND WHITE COLOR PRESENT IN HYDROPHOBIC REGIONS

The contour map shows a big purple region at the lower position of the pyridine ring, which is considered as the unfavorable region for hydrogen bond donor groups. The CoMSIA hydrogen-bond acceptor contour map shows a large magenta region located at the same position as the purple region of the contour map, indicating this as a favorable region for hydrogen bond acceptor. A large magenta contour and a medium sized red contour is present. A large violet color contour is present above the Nitrogen group. The presence of –NH group on this red contour is responsible for the favorable hydrogen bond acceptor regions on the molecule. Donor and acceptor contour maps are represented in **Fig. 5d** and **5e.**
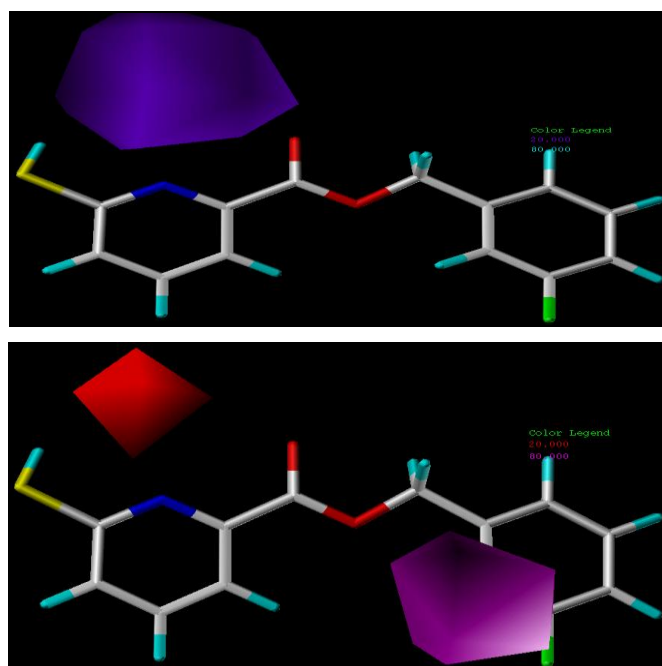

FIG. 5d: COMSIA CONTOUR MAPS ARE SHOWN IN THE PRESENCE OF THE MOST POTENT COMPOUND 16. LARGE VIOLET COLOR CONTOUR IS PRESENT INDICATES DONOR GROUP. FIG 5e. MEGENTA AND RED COLOR ARE PRESENT IN THE ACCEPTOR GROUP.

Docking results:

The most active compound 16 along with the remaining 63 molecules was docked into receptor site by using FlexX. The crystal structure (PDB ID: 1HFC) was used. The ligand with all water molecules was deleted and Gasteiger-Hückel charges were assigned. Then the structure was minimized using the conjugate gradient algorithm for 10,000 steps with no initial optimization, using Tripo's force field**.** Cut-off was set to 15Å and a distance dependent dielectric constant was employed. All atoms of the protein were treated as aggregates, with the exception of those within the 15Å radius of the bound ligand.

The ligand was pre-processed before docking calculations by giving charges according to the Gasteiger-Hückel method followed by energy minimization with 10,000 iterations of conjugate gradient algorithm using Tripo's force field. Using the FlexX module in the SYBYL 6.7 package, the ligand was docked into both the crystal structure and the relaxed one. For both structures the active sites include all residues within 15Å radius of the bound ligand and metals. Other functions were set to default values. All the molecules docking scores are given in the **Table 2.**

CONCLUSION: In the present study, the 3D QSAR, CoMFA, CoMSIA analysis was applied to predict the activity of pyridinone compounds. These QSAR, CoMFA, CoMSIA models gave a good statistical results in terms of q^2 and r^2 values. Both CoMFA and CoMSIA models show good correlation between observed and predicted inhibitory potencies against MMP-12, as indicating r^2_{cv} of 0.555 for CoMFA and of 0.550 for CoMSIA. Both the donor and acceptor show the significance of hydrogen bond interactions between MMP-12 enzyme and ligands. All of the constructed models possessed good internal and external consistency and showed statistical significance and predictive abilities. Both the predictive evaluation and the contour map analysis accorded well the experimental interaction mode of the first marked MMP inhibitors.

REFERENCES:

1. Divoux A. and Clement K: Architecture and the extracellular matrix: the still unappreciated components of the adipose tissue. Obes Rev 2011; 12: e494-e503.
2. Hulmes DJS: Building collagen molecules, fibrils, and suprafibrillar structures. J Struct Biol 2002; 137: 2-10.
3. Kielty CM, Sherratt MJ and Shuttleworth CA: Elastic fibres. J Cell Sci 2002; 115: 2817 2828.
4. Romberger DJ: Fibronectin. Int J Biochem Cell Biol 1997; 29: 939-943.
5. Ruoslahti E: Fibronectin and its receptors. Annu Rev Biochem 1988; 57: 375-413.
6. Potts JR and Campbell ID: Fibronectin structure and assembly. Curr Opin Cell Biol 1994; 6648-655.
7. Christiaens V and Lijnen HR: Role of the fibrinolytic and matrix metalloproteinase systems in development of adipose tissue. Arch Physiol Biochem 2006; 112: 254-259.
8. Shapiro SD: Matrix metalloproteinase degradation of extracellular matrix: biological consequences. Curr Opin Cell Biol 1998; 10: 602-608.
9. Murphy G, Hembry RM: Proteinases in rheumatoid arthritis. J Rheumatol Suppl. 1992; 32:61-64.
10. Overall CM, Wiebkin OW, Thonard JC: Demonstration of tissue collagenase activity *in vivo* and its relationship severity inhumangingiva. J Periodontal Res. 1987; 22:81-88.
11. Peress N, Perillo E, Zucker S: Localization of tissue inhibitor of matrixmetalloproteinases in Alzheimer's disease and normal brain. J Neuropathol Exp Neurol. 1995; 54:16-22.
12. Clark M, Cramer RD and Opdenbosch NV: Validation of the general purpose tripos 5.2 force field. J Comput Chem. 1989; 10:982-1012.
13. Cramer RD, Patterson DE, Bunce JD: Comparative molecular field analysis (CoMFA) 1 Effect of shape on binding of steroids to carrier proteins. J Am Chem Soc. 1988; 110:5959-5967.
14. Klebe G, Abraham U, Mietzner T: Molecular similarity indices in a comparative analysis (COMSIA) of drug molecules to correlate and predict their biological activity. J Med Chem. 1994; 37:4130-4146.
15. Ryuji H, Xiaomin Jin, Gregory Cook R: Synthesis and evaluation of novel heterocyclic MMP inhibitors. Bioorg Med Chem Lett.2007; 17:6864-6870
16. Weerasak S, Patcharawee N, Jirapm U: 3D-QSAR investigation of synthetic antioxidant derivatives by molecular field analysis. Int J Mol Sci. 2008; 9:235-246
17. Cramer RD, Bunce JD, Patterson DE,and Frank IS: Cross-validation, bootstrapping and partial least squares compared with multiple regression in conventional QSAR studies. Quant Struct Act Relat 1988; 7: 18-25.
18. Geladi P, Kowalski B: Partial least-squares regression: A tutorial. Analytica Chimica Acta. 1986; 185: 1-17
19. Kramer B, Metz G, Rarey M,and Lengauer T:Ligand docking and screening with FlexX. Med Chem Res. 1999; 9: 463-478.
20. Gilbert KM, Skawinski M, Misra KA, Paris NH, Buono aik RA, Deutsch HM and Venanzi CA: Conformational analysis of methylphenidate: comparison of molecular orbital and molecular mechanics methods. J Comput Aided Mol Des. 2004; 18:719-724.

This article can be downloaded to **ANDROID OS** based mobile. Scan QR Code using Code/Bar Scanner from your mobile. (Scanners are available on Google Playstore)